ACS APPLIED MATERIALS & INTERFACES

Locally Saturated Ether-Based Electrolytes With Oxidative Stability For Li Metal Batteries Based on Li-Rich Cathodes

John Holoubek,[†] Haodong Liu,[†] Qizhang Yan,[†] Zhaohui Wu, Bao Qiu, Minghao Zhang, Sicen Yu, Shen Wang, Jianbin Zhou, Tod A. Pascal, Jian Luo, Zhaoping Liu, Ying Shirley Meng, and Ping Liu*

Cite This: https://doi.org/10.1021/acsami.3c07224

Read Online

ACCESS | Metrics & More | Article Recommendations | Supporting Information

ABSTRACT: Li metal batteries applying Li-rich, Mn-rich (LMR) layered oxide cathodes present an opportunity to achieve high-energy density at reduced cell cost. However, the intense oxidizing and reducing potentials associated with LMR cathodes and Li anodes present considerable design challenges for prospective electrolytes. Herein, we demonstrate that, somewhat surprisingly, a properly designed localized-high-concentration electrolyte (LHCE) based on ether solvents is capable of providing reversible performance for Li‖LMR cells. Specifically, the oxidative stability of the LHCE was found to heavily rely on the ratio between salt and solvating solvent, where local-saturation was necessary to stabilize performance. Through molecular dynamics (MD) simulations, this behavior was found to be a result of aggregated solvation structures of Li$^+$/anion pairs. This LHCE system was found to produce significantly improved LMR cycling (95.8% capacity retention after 100 cycles) relative to a carbonate control as a result of improved cathode-electrolyte interphase (CEI) chemistry from X-ray photoelectron spectroscopy (XPS), and cryogenic transmission electron microscopy (cryo-TEM). Leveraging this stability, 4 mAh cm^{-2} LMR‖2× Li full cells were demonstrated, retaining 87% capacity after 80 cycles in LHCE, whereas the control electrolyte produced rapid failure. This work uncovers the benefits, design requirements, and performance origins of LHCE electrolytes for high-voltage Li‖LMR batteries.

KEYWORDS: Li metal battery, Li-rich cathode, battery electrolyte, solvation, solid-electrolyte interphase, cathode-electrolyte interphase
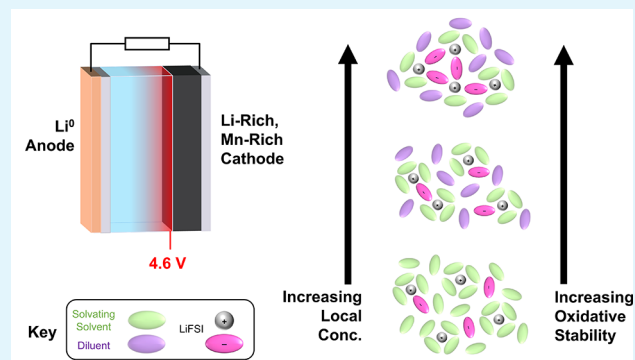
INTRODUCTION

The advent of energy-dense Li-ion batteries (<250 Wh kg^{-1}) has resulted in the deployment of portable electronic devices at an unprecedented scale. However, to continue supporting these ever-improving devices and to ensure the adoption of electric vehicles, improved energy densities are required. Li metal batteries, which replace the conventional graphite anode with Li metal, promise cell-level energy densities approaching 500 Wh kg^{-1}.[1] However, achieving such lofty metrics with conventional cathodes requires advancements in currently achievable electrode and electrolyte loading, inactive material content, all the while maintaining excellent Li metal anode reversibility. Additionally, these projected metrics rely heavily on high-Ni transition metal oxide cathodes, which are becoming less tenable due to supply chain and sustainability concerns.[2] The employment of alternative cathodes which provide improved capacity output with less reliance on Ni and Co is therefore paramount.

Li-rich, Mn-rich (LMR) layered oxide cathodes that produce reversible capacity via both cationic and anion redox present an enormous opportunity to fill this void. These layered cathode materials commonly boast atomic Mn contents >50% of the

total transition metal count which produces a reduction in cost compared to mainstream Ni-rich cathodes.[3,4] Moreover, LMR systems exhibit high specific capacities of >250 mAh g^{-1}, alleviating the energy density losses associated with other low-cost materials such as LiMnO$_2$ (LMO).[5] As there is ever-increasing interest in pushing cell energy densities beyond their current limits for mass-market applications, LMR cathodes are therefore ideal to pair with high-energy anodes such as Li metal. To demonstrate this, we project the energy density of 5 Ah pouch cells through a model described in the Supporting Information. As shown in Figure 1, Li metal batteries employing LMR cathodes promise energy densities far exceeding cells composed of LiNi$_{0.8}$Mn$_{0.1}$Co$_{0.1}$O$_2$ (NMC 811), LiNi$_{0.333}$Mn$_{0.333}$Co$_{0.333}$O$_2$ (NMC 111), and LiFePO$_4$ (LFP). Further, they provide a viable route to achieving
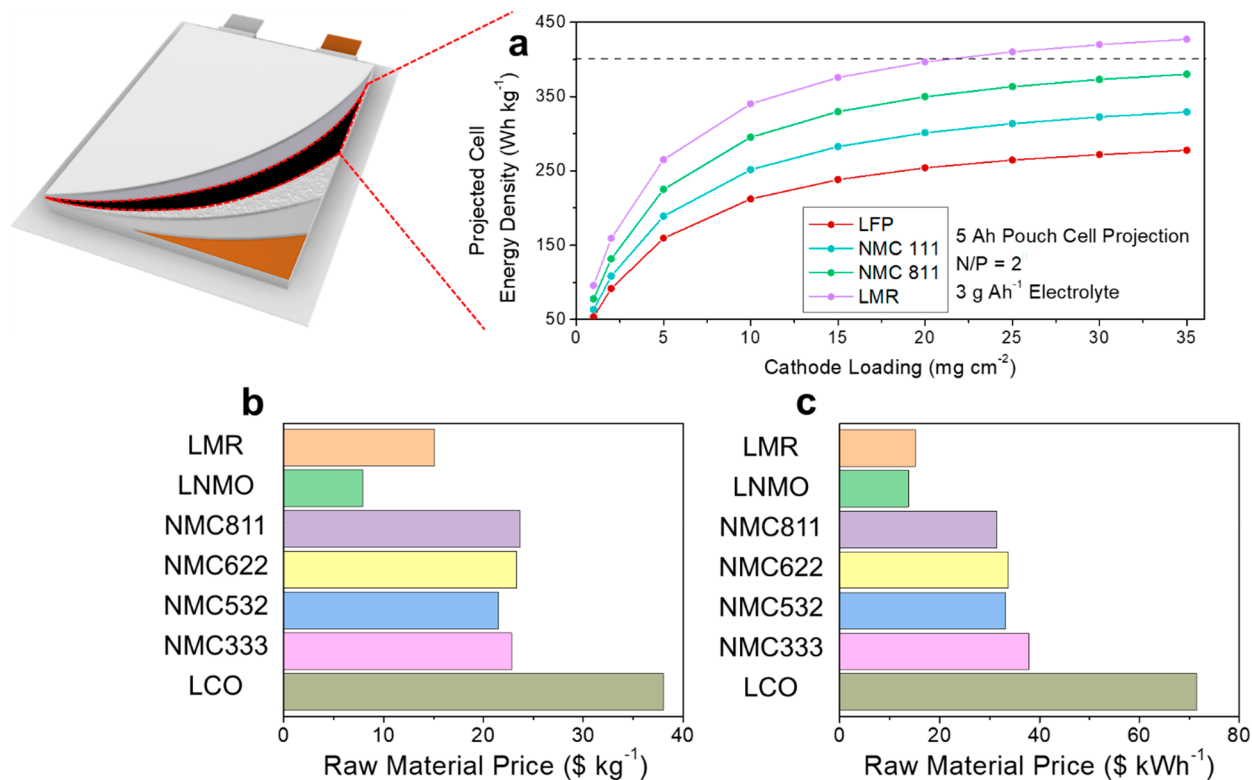
Figure 1. Impact of cathode chemistry on the energy density of Li metal batteries. (a) Projected energy density of 5 Ah cells with N/P = 2 and 3 g Ah^{-1} electrolyte based on a pouch-cell model. Calculated raw materials cost of cathode materials of interest based on January 2023 commodity prices in (b) USD kg^{-1}, (c) USD kWh^{-1}. We note that applying reduced inactive cell components, N/P ratio, and electrolyte loadings can yield energy densities >500 Wh kg^{-1} as previously calculated.[1]

>400 Wh kg^{-1} at the cell-level with the currently achievable electrolyte loading of 3 g Ah^{-1} and N/P ratio of 2. LMR cathodes promise to achieve such energy densities with minimal reliance on Ni and Co, with a calculated raw materials cost of <16 $ kg^{-1} and <20 $ kWh^{-1}, which rivals high-voltage spinel.

The high capacity of LMR cathodes are generated through both the redox of transition metals *and* Li-coordinated oxygen within the host, promoting surface reorganization and gas formation.[5−10] Accordingly, the specific capacity of LMR cathodes have been observed to degrade severely with cycling. However, recent work has suggested that the electrolyte composition may significantly enhance said stability, which is largely a result of improved cathode-electrolyte interphase (CEI) chemistry.[11,12] Despite this promise, the library of available electrolytes compatible with LMR systems is still relatively narrow given the oxidative stability requirements must exceed 4.6 V vs Li/Li$^+$. Moreover, application of LMR cathodes in Li metal batteries places a similarly stringent stability criteria for the electrolyte and the Li metal anode. The advent of stable electrolytes, which endow stability on both LMR cathodes and Li metal anodes, is therefore paramount.

The mainstream carbonate electrolyte, such as those based on EC/DMC (ethylene carbonate/dimethyl carbonate), has demonstrated high voltage stability up to 4.8 V.[13] However, despite their apparent oxidative stability, the cathode-electrolyte interphase formed in such systems tend to be insufficient for LMR cycling. Moreover, the Coulombic efficiency (CE) for Li metal cycling in these electrolytes tend to hover near ∼90%, an untenable value for Li metal full cell operation.[14] While conventional ether electrolytes, such as those based on 1,2-dimethoxyethane (DME) and low-concentrations of lithium bis(fluoro sulfonyl)imide (LiFSI) are known to stabilize the Li metal anode, they face challenges in oxidative stability on the cathode.[15,16] The advent of localized-high-concentration electrolytes (LHCE) systems have made significant advances in oxidative stability, enabling the application of standard transition metal oxide cathodes.[17,18] However, the only LHCE systems applied to Li‖LMR systems have so far been based on carbonate solvents.[12]

In this work, we find that, unexpectedly, ether-type LHCE electrolytes based on LiFSI, DME, and bis(2,2,2-trifluoro ethyl)ether (BTFE), simultaneously support the operation of the Li$_{1.143}$Ni$_{0.136}$Co$_{0.136}$Mn$_{0.544}$O$_2$ LMR cathode and the Li metal anode. We demonstrate that the ratio between LiFSI, DME, and BTFE is crucial to achieve the oxidative stabilities necessary for LMR operation, and relatively unimportant for stabilization of Li metal cycling. The origin of this behavior was probed through molecular dynamics (MD), which revealed that the statistical prevalence of multianion Li$^+$ "aggregates" described the oxidative behavior. The highly aggregated LHCE was then applied to LMR half cells and LMR‖limited Li full cells, where it was found to endow exceptionally stabilized performance relative to the carbonate control. This performance was found to largely be a result of interphase CEI composition, as revealed by cryogenic transmission electron microscopy (cryo-TEM), and X-ray photoelectron spectroscopy (XPS). This work demonstrates the viability of LHCE in Li‖LMR full batteries, outlines the relevant electrolyte design parameters necessary to achieve stability, and provides a mechanistic analysis of their improved behavior.
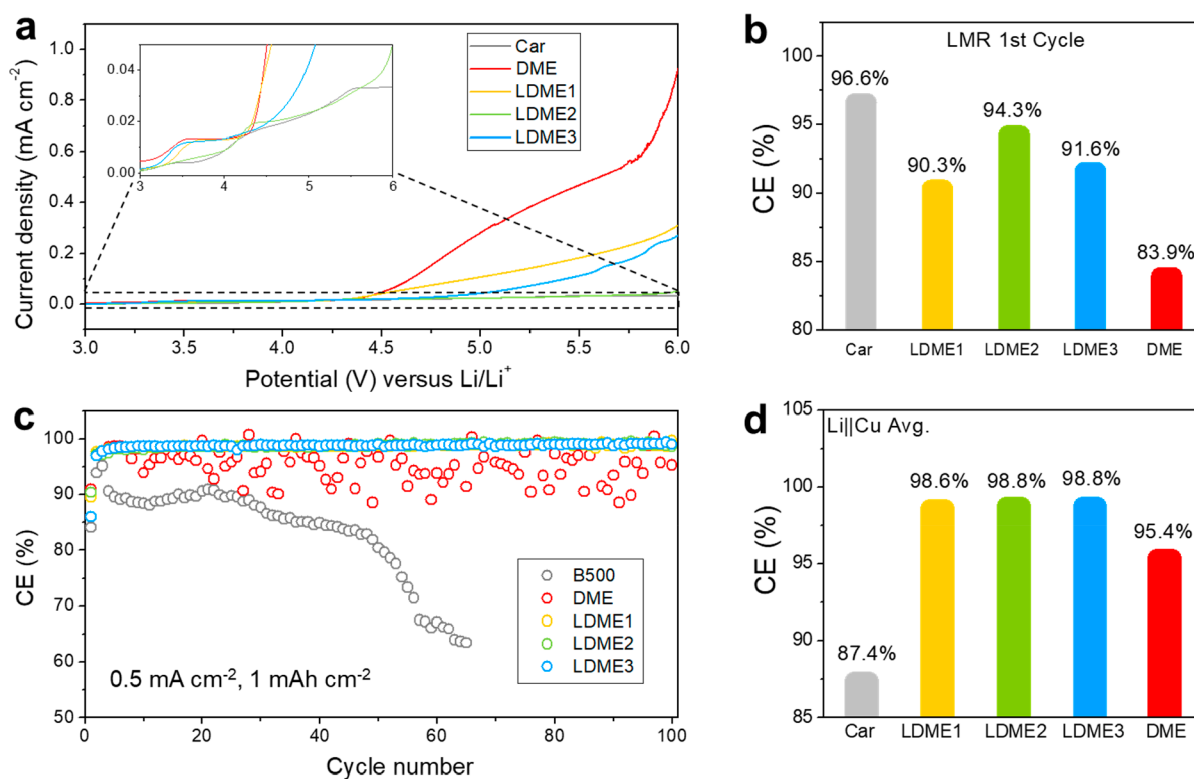
Figure 2. Electrolyte stability tests. (a) Oxidation stabilities for different electrolytes as evaluated on Al electrode at a scan rate of 5 mV s^{-1}. (b) First cycle Coulombic efficiencies of Li‖LMR half cells in different electrolytes when cycled at C/20 from 2 to 4.6 V. (c) Coulombic efficiencies of Li‖Cu cells over the course of 100 cycles in different electrolytes, 0.5 mA cm^{-2} for 1 mAh cm^{-2}. (d) Average Coulombic efficiencies of Li‖Cu cells in different electrolytes, averaged over 100 cycles for LHCE and 50 for car. Car is 1.2 M LiPF$_6$ in EC/EMC (Vol:Vol = 3:7), DME is 1 M LiFSI DME, LDME1 is LiFSI-DME-BTFE 1−1.6−3.2 (by mol), LDME2 is LiFSI-DME-BTFE 1−1.1−5.0 (by mol), and LDME3 is LiFSI-DME-BTFE 1−1.6−7.1 (by mol).

RESULTS AND DISCUSSION

To better understand these electrolyte design requirements for Li‖LMR batteries, we compare a conventional carbonate electrolyte, 1.2 M LiPF$_6$ in EC/ethyl methyl carbonate (EMC) 3:7 (vol), to a conventional ether electrolyte, 1 M LiFSI DME and a variety of LHCE systems based on LiFSI, DME, and BTFE. BTFE is known to act as a "diluent" in such systems, which reduces the overall solution viscosity, but does not meaningfully contribute to Li$^+$ solvation due to its heavy fluorination.[19] Accordingly, the LHCE system is entirely reliant on DME to solvate salt, and thus the ratio between DME and LiFSI primarily dictates the local solvation environment of Li$^+$ irrespective of BTFE content. However, the diluent in LHCE systems has been proposed to contribute toward the SEI and CEI, which must be considered.[19] Regarding solvation, it is useful to define the "local concentration" of a given LHCE as the concentration of LiFSI only with respect to the solvating solvent (in this case DME), which dictates the equivalent high-concentration electrolyte one would expect the LHCE solvation environment to resemble.[20−23] Similarly, a "locally saturated" solution refers to a system in which the LiFSI/solvating solvent ratio is at its maximum as dictated by the solubility limit.

To investigate the influence of these effects, we compare LiFSI-DME-BTFE systems of molar ratios 1−1.6−3.2 and 1−1.1−5.0 (by mol) referred to as "LDME1" and "LDME2". Despite the negligible influence of BTFE on solvation, the relative concentration of fluorinated diluents have been shown to have a significant effect on Li$^+$ transport in the system, and

to contribute to the solid-electrolyte interphase.[23,24] Hence, we also compare these two LCHE systems to one with elevated BTFE composition, LiFSI-DME-BTFE 1−1.6−7.1 (mol), referred to as "LDME3". Performance effects arising from differences in local concentration, e.g., degree of ion-pairing and salt aggregation would be observed via differences in performance between LDME1 or 3 and LDME2, whereas the effect of global salt concentration and/or BTFE content would produce differences in performance among all 3 systems, especially LDME1 and LDME3.

To approximate the oxidative stability of these electrolytes, we apply them to linear-scan voltammetry in Li‖Al cells. As shown in Figure 2a, 1 M LiFSI (LiFSI:DME ∼ 1:11) was shown to decompose readily beginning at ∼4.4 V, behavior that is known to have limited the application of conventional ether electrolytes with transition metal oxide cathodes.[15,16] However, when the LiFSI:DME ratio is increased to 1:1.6 (∼6 M local concentration) in LDME1, this decomposition is significantly suppressed, reaching 0.11 mA cm^{-2} at 5.0 V vs Li/Li$^+$ as opposed to 0.29 mA cm^{-2}. Interestingly, this decomposition is also reduced by maintaining the same LiFSI:DME ratio, but increasing the BTFE content from LDME1 to LDME3, which supports previous observations that diluent plays a role in oxidative stability. However, this influence was found to be of little consequence when compared to increased LiFSI:DME ratio, where the LDME2 electrolyte displayed negligible parasitic current until ∼5.9 V, comparable to the carbonate electrolyte. To provide a more meaningful measure of this stability, LMR‖Li half cells were
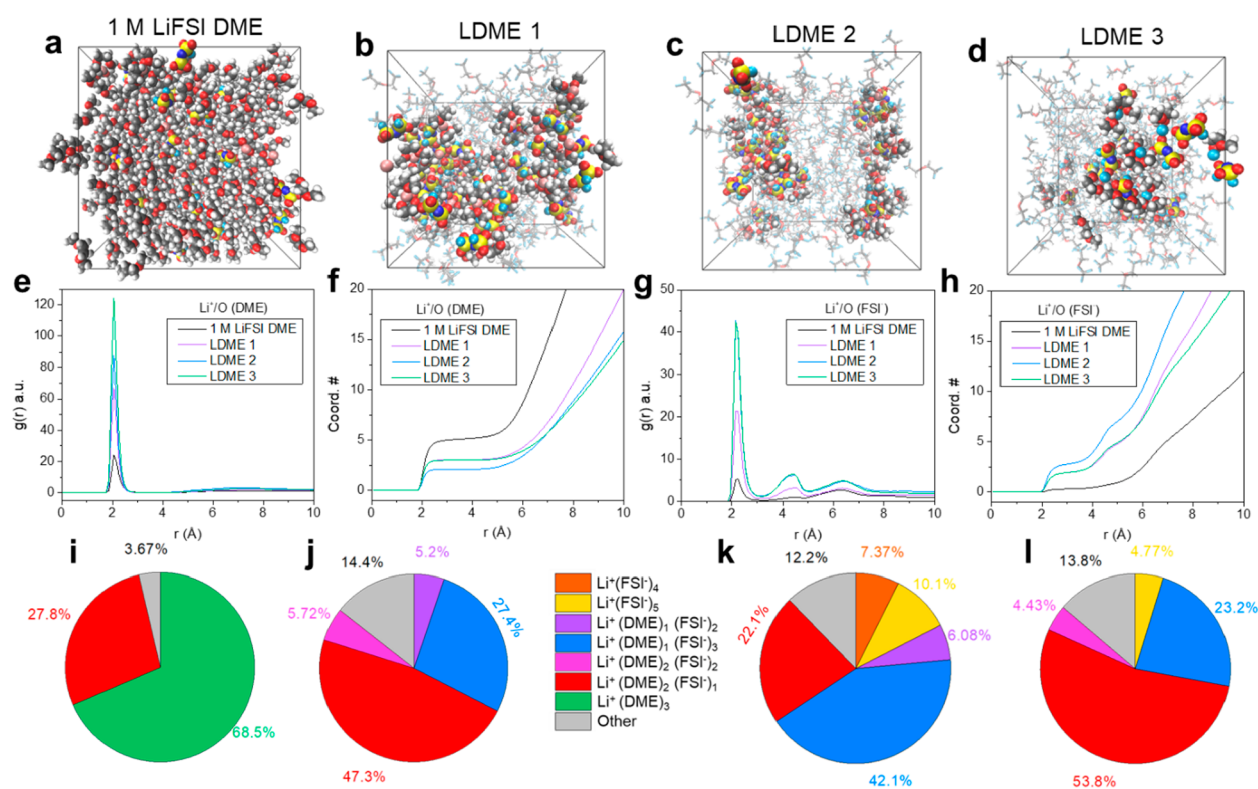
Figure 3. Molecular dynamics simulations of ether electrolytes of interest. (a–d) Final MD snapshot of the DME, LDME1, LDME2, and LDME3, respectively. Color: Li, pink; O, red; C, gray; H, white; N, blue; S, yellow; and F, cyan. (e) Radial distribution functions (RDFs) of the DME oxygen with respect to Li⁺. (f) Integrated RDFs of the DME oxygen atoms, representing the lithium coordination number. (g) RDFs of the FSI oxygen with respect to Li⁺. (h) Integrated RDFs of the FSI⁻ oxygen atoms, representing the lithium coordination number. (i–l) Solvation distribution analysis of the Li⁺ atom in DME, LDME1, LDME2, and LDME3, respectively.

assembled with each electrolyte. As shown in Figure 2b, the first cycle Coulombic efficiencies (CEs) of each electrolyte match the trends predicted by LSV, with their profiles shown in Figure S1. However, despite their initial efficiencies, the largely organic CEI produced by carbonates is known to be disadvantageous for long-term cathode cycling, which will be investigated for the LMR system later in this work.[25]

To ensure compatibility with both the LMR cathode and the Li metal anode, the electrolytes of interest must demonstrate improved reductive stability in addition their oxidative behavior. Hence, the electrolytes were applied in Li‖Cu cells to measure their CE for Li metal cycling at 0.5 mA cm⁻², and 1 mAh cm⁻² over long time scales. As shown in Figure 2c, despite its apparent oxidative stability, the carbonate electrolyte was found to produce an average CE of 87.4% for Li metal cycling, which then rapidly degraded after ~50 cycles. This behavior has been previously demonstrated to be a result of electrolyte exhaustion, and is seen widely in carbonate-based electrolytes.[26] The 1 M LiFSI DME system, by contrast, shows a significantly improved average CE of 95.4%, but is still insufficient in providing viable reversibility for full cell applications. The LHCE systems, on the other hand, were all found to demonstrate remarkable CEs for Li metal cycling, displaying 98.6, 98.8, and 98.8% averages over the initial 100 cycles in LDME1, LDME2, and LDME3, respectively. We note that these are diminished by the conditioning process typically observed at low plating capacity, where similar systems are known to produce >99% CE values post conditioning.[18] Unlike the oxidative stability trends, we find that the composition of LiFSI, DME, and BTFE were relatively

unimportant for such cycling efficiencies, indicative of the inherent reductive stability of ether solvents in the presence of fluorine-donating FSI⁻.[27]

The influence of Li⁺ solvation within the electrolyte has been widely demonstrated to dictate electrochemical stability and solid interphase formation.[28,29] To provide a molecular understanding of the structures present in each electrolyte of interest, we apply MD simulations (Figure 3a–d). Specifically, to understand the effects of LHCE composition on said structure, and the resulting electrochemical performance, we compare 1 M LiFSI DME with the LDME1, LDME2, and LDME3 solutions (Methods shown in the Supporting Information). The radial distribution function (RDF) with respect to Li⁺ ions in solution is widely used to assess the statistically distribution of solvation states, which we analyze over 12.5 ns of production dynamics. The RDFs for DME and FSI⁻ oxygen atoms, the primary solvating species, are shown in Figure 3e and g, respectively. As these profiles represent the statistical probabilities of certain states without consideration of the total concentration of various electrolyte species, we instead make conclusions based on their associated integrals, which directly respond to the coordination number of each species to Li⁺ (Figure 3f, h). Through this analysis, we observe that the solvation structure of 1 M LiFSI DME is dominated by solvent, generally referred to in the literature as a solvent-separated ion-pair structure (SSIP). However, this structure undergoes a distinct shift in the LHCE systems, where the FSI⁻ anion participates heavily in solvation. The *average* solvation structure of 1 M LiFSI DME is predicted to be Li⁺(DME)₂.₆(FSI⁻)₀.₃₂, whereas the average structures of
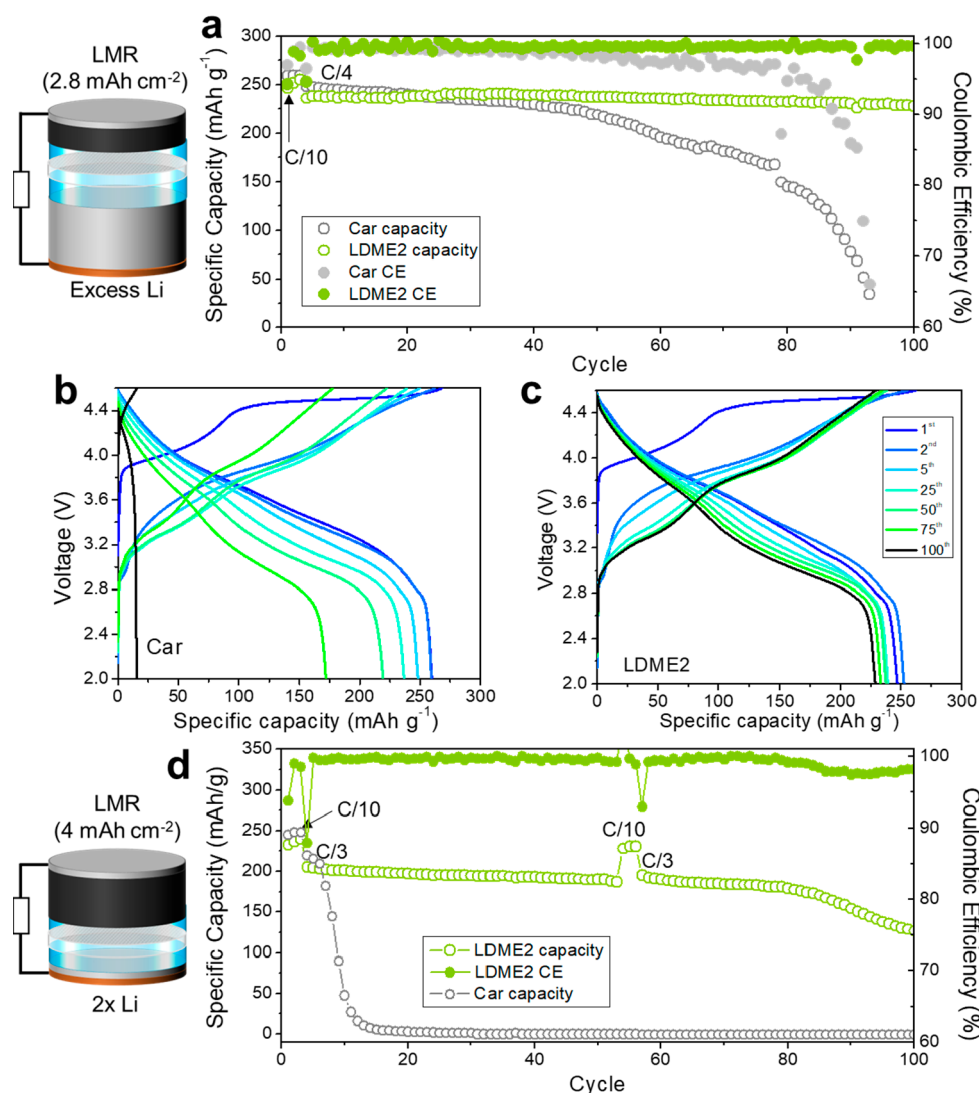
Figure 4. Electrochemical cycling data of LMR‖Li cells applying LDME and car electrolytes. (a) LMR half cell cycling data with 2.8 mAh cm^{-2} LMR electrodes from 2 to 4.6 V. Voltage profiles of half cells utilizing (**b**) car and (**c**) LDME2 electrolytes. (d) Full cell cycling of 4 mAh cm^{-2} LMR cathodes paired with a preplated 2× Li metal anode cycled from 2 to 4.6 V.

LDME1, LDME2, and LDME3 are predicted to be $Li^+(DME)_{1.5}(FSI^-)_{1.9}$, $Li^+(DME)_{1.0}(FSI^-)_{2.8}$, and $Li^+(DME)_{1.5}(FSI^-)_{1.9}$, respectively.

Beyond the average solvation structure, we take 250 "snapshots" of the local structure (within 3 Å) of each Li$^+$ atom (every 0.1 ns), in order to build a statistical distribution of states in a similar method to our previous work.[20] These distributions are shown in Figure 3i−l. When analyzed in this fashion, it is found that the SSIP $Li^+(DME)_3$ structure is prominently displayed in 1 M LiFSI DME, representing 68.5% of the states, compared to a 27.8% prevalence of $Li^+(DME)_2(FSI^-)_1$ structures, commonly referred to as "contact-ion pairs" (CIP). Aside from displaying a higher degree of ion-pairing in the structures, we also find that the LHCE systems show high probabilities for ion "aggregate" (AGG) structures, in which Li$^+$ is coordinated by >1 FSI$^-$. Specifically, LDME1 was found to demonstrate a CIP structure 47.3% of the time, whereas AGG structures accounted for ∼38.3% and no statistically significant sign of SSIP structures. LDME3, while showing slight differences in the speciation of specific AGG species, the overall prevalence of CIP and AGG

structures were found to be relatively comparable at 53.8 and 32.4%, respectively. We note that the majority of the structures comprising "other" are also AGG in nature, but did not meet the 3% statistical relevance criteria to be specified discretely. LDME2, on the other hand, was found to be dominated by AGG structures, showing 22.1 and ∼65.7% CIP and AGG prevalence, respectively. As the parasitic decomposition of ether solvent is known to limit its high-voltage performance, and is known to be suppressed by the reduction in free solvent and anion-derived CEI compositions, we conclude that the increase in AGG species shown in LDME2 is responsible for its improved oxidative stability.

To determine the impact of LDME2 over the conventional carbonate electrolyte on the cycling performance of the aforementioned LMR cathode, we assembled 2.8 mAh cm^{-2} LMR‖Li half cells utilizing each electrolyte (Figure 4a schematic). When cycled at a C/4 rate from 2 to 4.6 V, we find that the LMDE2 system produces remarkable LMR cycling stability relative to the carbonate system. Specifically, the LMR cathode was found to retain 97% capacity retention after 100 cycles in LDME2, whereas the LMR cathode in
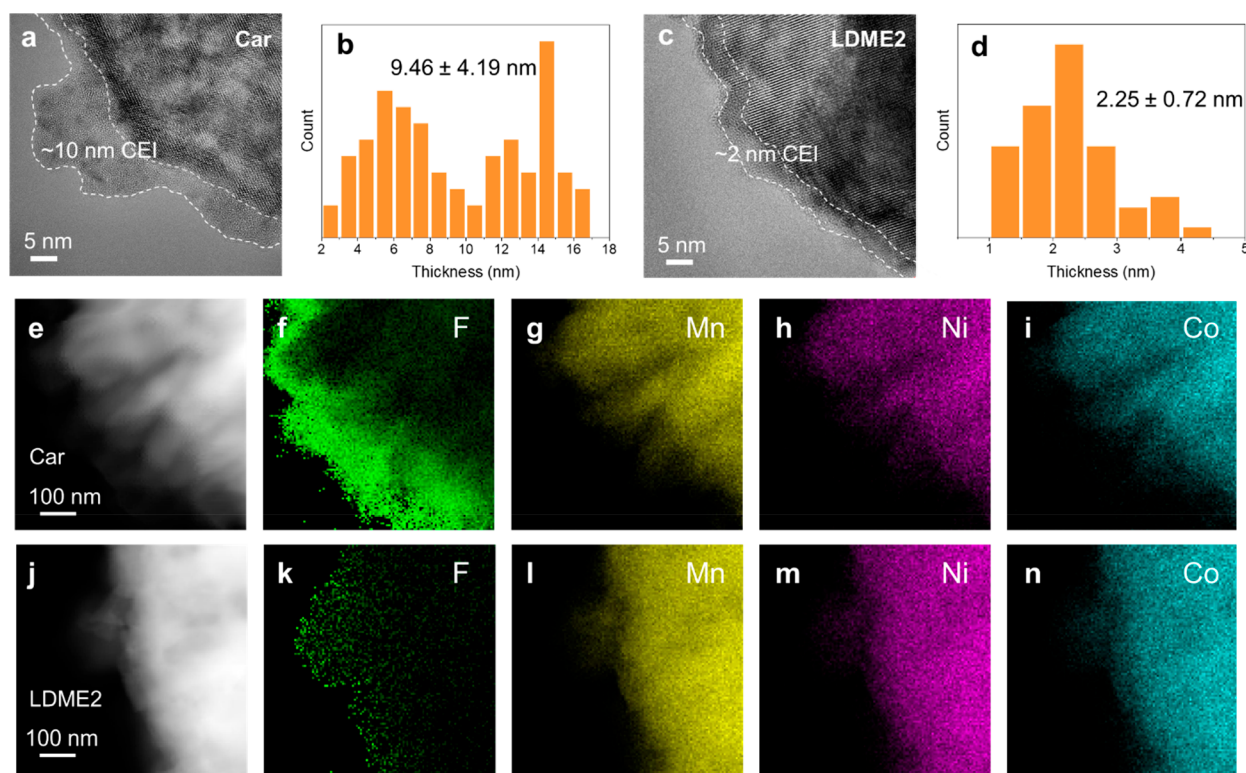
Figure 5. Cryo-TEM of the CEI formed on LMR cathodes after 100 cycles in half cells. (a) TEM micrograph of CEI formed in carbonate and (b) the statistical distribution of CEI thickness. (c) TEM micrograph of CEI formed in LDME2 and (d) the statistical distribution of CEI thickness. Cryo-STEM-EDS of the CEI formed in each electrolyte. (e) Cryo-STEM micrograph, and associated (f) F, (g) Mn, (h) Ni, and (i) Co maps of the carbonate CEI. (j) Cryo-STEM micrograph, and associated (k) F, (l) Mn, (m) Ni, and (n) Co maps of the LDME2 CEI.

carbonate retained only 69% after 75 cycles, after which the capacity dropped precipitously, likely due to electrolyte exhaustion as a result of poor Li metal compatibility (Figure 4a).[26] This anode limitation is supported by the discharge curves for the carbonate system shown in Figure 4b, where a sharp decrease in voltage toward the end of discharge indicates depletion of the Li reservoir. Before this depletion, the cell degradation was gradual and seen uniformly throughout the voltage curve, indicative of cathode degradation. The enhanced cycling stability of LDME2 was also found to be accompanied by improved output voltage retention, as shown in 4c. Given the comparable intrinsic oxidative stability between LDME2 and the carbonate system, it is likely that the improved stability of LMR cycling in LDME2 is a result of improved CEI composition. While the enhanced capacity retention of LMR in LDME2 at high discharge rates suggests a reduced interphasial impedance (Figure S2) the composition and morphology of this interphase must be understood, and will be further discussed below.

As high-energy density full cells require limited Li anodes, the Li metal cycling stability of the electrolyte is also of high interest. Hence, we examine the cycled Li counter electrodes after 100 half cell cycles via scanning electron microscopy (Figure S3). We find in both top-view and cross-sectional imaging that the Li cycled in the carbonate electrolyte shows substantially more porosity, where the initial 250 μm counter electrode only displayed ∼40 μm uncycled Li compared to 178 μm uncycled Li in LDME2 (Figure S3b, d). The extreme pulverization and dendritic nature (Figure S3a) observed in carbonate has been previously observed to be a consequence of poor cycling stability, and supports the CE observations made

previously. This improved Li metal morphology is also observed in tandem with a increase in Fluorinated species in the SEI via XPS. As shown in Figures S5 and S6, the LDME2 system produced abundant LiF, SO_xF_y, and C−F species derived from FSI$^-$ and BTFE decomposition which are maintained after 100 cycles in addition to an increased prevalence of Li−F. These species have been widely observed in sulfonylimide-based electrolytes and are commonly associated with the highly reversible performance they demonstrate.[19,30] Though the carbonate system was also found to produce LiF, its otherwise organic and PO_xF_y-containing SEI was evidently insufficient for long-term reversible cycling, as evidenced by the existence of polycarbonate species derived from reductively unstable EC.

To further demonstrate the beneficial effect of the LDME 2 electrolyte on the LMR and Li anode in tandem, we assembled 4 mAh cm^{-2} LMR ∥ 2x Li (N/P ratio = 2) full cells (Figure 4d schematic). These cells were also cycled between 2 and 4.6 V in a manner to capture capacity fade due to losses in kinetics at elevated rate ($C/3$) and any materials-level capacity fade by cycling again at $C/10$ after 50 cycles. When cycled, it was found that the full cell applying LDME2 produced negligible fade between the $C/10$ cycling capacities before and after 50 $C/3$ cycles, whereas the 87% output capacity was retained after 80 cycles at $C/3$ (Figure 4d). Significant capacity fade was observed after 80 cycles, which is likely due to depletion of the excess Li metal reservoir, as shown in the Voltage curves and $dQ\ dV^{-1}$ profiles, which feature a sharp reduction in capacity at the end of discharge. On the other hand, the carbonate electrolyte was found to produce rapid failure, displaying negligible capacity after 15 cycles with the aforementioned
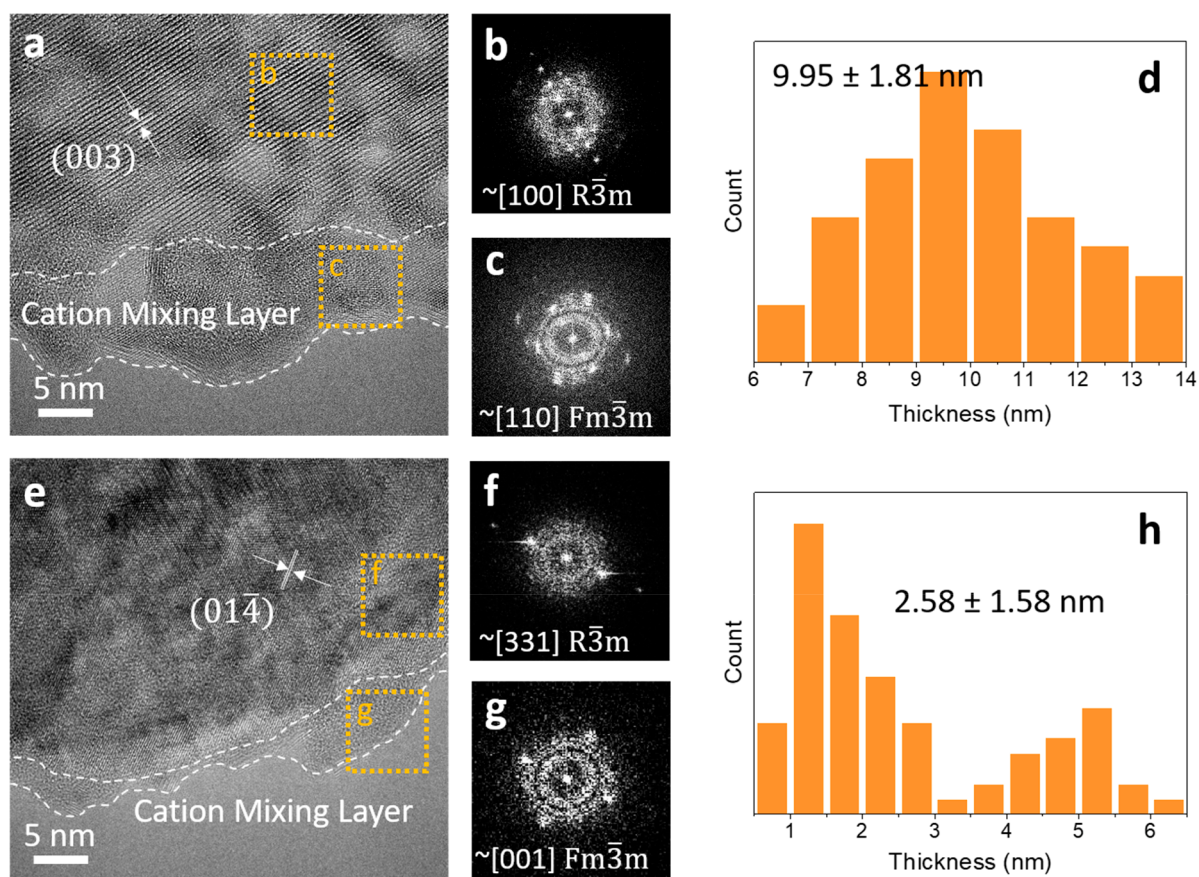
Figure 6. TEM of the cation mixing layer formed on the surface of LMR cathode particles after 100 cycles in half cells. (a) TEM micrograph of CEI formed in carbonate and the FFT patterns of (b) bulk particle compared with (c) the cation mixing layer. (d) statistical distribution of cation mixing layer thickness. (e) TEM micrograph of CEI formed in LDME2 and the FFT patterns of (f) bulk particle compared with (g) the cation mixing layer. (h) Statistical distribution of cation mixing layer thickness.

characteristic behavior of Li anode depletion (Figure 4d, Figure S4).

Though the improved Li metal cycling behavior provided by LHCE systems is well known, their stabilization of high-voltage LMR cathodes is surprising given the oxidative instability of ether solvents and sulfonylimide anions.[16,31,32] To better understand this, we first conducted XPS on the cycled LMR cathodes after 1 and 100 cycles in half cells. As shown in Figures S7 and S8, the LMR cathode cycled in carbonate showed significant variance between initial formation and 100 cycles, where significant relative increases in Li–F, and most notably C–O contributing peaks were observed (Figure S7a, c). Though Li–F has been previously observed to have a beneficial impact on electrochemical stability, we interpret its increased prevalence over the cycling duration in tandem with the increased prevalence of organic species to indicate continued parasitic decomposition. On the other hand, we observe minimal variance in the carbon-containing CEI constituents formed in LDME2 over 100 cycles. Though a slight increase in SO_x-F_y species was observed, the well-established passivating benefits of these constituents suggests improved passivation (Figure S8b, d). Hence, the XPS data indicate that the CEI produced at the LMR cathode in LHCE is superior for long-term cycling than that of the carbonate system.

To study the CEI morphology in different electrolytes without electron beam damage, the cycled LMR cathodes were characterized with cryogenic transmission electron microscopy (cryo-TEM).[33,34] After 100 cycles in the carbonate electrolyte, a nonuniform amorphous CEI with a thickness of 9.46 ± 4.19 nm was observed on the LMR surface as shown in Figure 5a cryo-TEM micrograph of a primary cathode grain. Figure 5f–i shows the low-magnification Cryo-STEM-EDX mapping of a secondary LMR particle. Excess fluorine characteristic X-ray signal was observed at the particle surface, which suggests the thick CEI layer formation from excessive electrolyte decomposition reaction. In contrast, the LMR cycled in LDME2 shows a more uniform and thinner CEI layer with 2.25 ± 0.72 nm thickness compared to the cathode cycled in baseline electrolyte as shown in Figure 5c and d. The improved CEI layer morphology was further confirmed with the low-mag EDX mappings in Figure 5k.

More evidence of improved interfacial stability with LDME2 electrolyte can be obtained from the formation of the surface rock-salt phase after prolonged cycling.[35] Figure 6 shows the TEM images and the corresponding bulk region and surface region fast Fourier transform (FFT) patterns of the cycled LMR electrode in carbonate and LDME2. In the carbonate electrolyte, the cycled LMR showed severe irreversible surface reconstruction from $R\bar{3}m$ layered structure to $Fm\bar{3}m$ rock-salt structure.[36,37] In this case, a surface rock-salt phase layer of 9.95 ± 1.81 nm was observed, which indicates severe interfacial side reactions. In comparison, the LMR cycled in LDME2 demonstrates a decreased surface rock-salt layer thickness of 2.58 ± 1.58 nm. Electrolyte decomposition at the LMR surface has been previously considered as a potential source of lattice-

O loss, which leads to subsequent Mn reduction and reorganization.[9] This mitigated surface reorganization and altered interphase chemistry may also relate to the recently demonstrated improvements in gas generation from LHCEs on Ni-based cathodes at high voltage.[38] These data, paired with the XPS investigation, indicate that the observed cycling improvement in LDME2 originates from its CEI chemistry.

CONCLUSION

In conclusion, we demonstrate that proper design of an LHCE electrolyte enables the reversible cycling of Li metal anodes and LMR cathodes simultaneously. While the inherent stability of LiFSI and DME was found to produce similarly reversible Li metal anode cycling performance regardless of LiFSI/DME ratio, we find that a locally saturated LHCE is necessary for oxidative stabilization >4.5 V, where the LMR cathode is cycled. Via MD simulations, this local saturation was found to result in a significant shift in solvation structure away from $Li^+(DME)_2(FSI^-)_1$ dominance and toward aggregates in which Li^+ pairs with multiple FSI^- anions. Despite similar oxidative stabilities vs blocking electrodes, we find that this locally saturated LHCE electrolyte provides significantly improved LMR cycling relative to a conventional carbonate electrolyte. This stabilization was found to be primarily a result of an improved CEI composition, which displayed reduced thickness and little compositional change over the 100 cycles and resulted in less cation reorganization at the cathode particle surface. The improved cathode interphase, in addition to the high Li metal anode reversibility provided by the LHCE system allowed for the reversible cycling of 4 mAh cm^{-2}, limited Li full cells capable of 100 cycles. This work demonstrates a viable route to high-voltage Li||LMR batteries while providing the design principles to do so and their chemical origins.

ASSOCIATED CONTENT

SI Supporting Information

The Supporting Information is available free of charge at https://pubs.acs.org/doi/10.1021/acsami.3c07224.

> Experimental methods including materials, electrochemical testing, characterization, molecular dynamics simulations, cell-level energy density and cathode cost projections; 1st cycle voltage curves of LMR half cells; variable discharge rate performance of LMR half cells; scanning electron microscopy of Li counter electrodes after cycling; voltage curves of LMR full cells with dQ dV^{-1} analysis; XPS of Li counter electrodes after 1 and 100 cycles; XPS of LMR counter electrodes after 1 and 100 cycles (PDF)

AUTHOR INFORMATION

Corresponding Author

  Ping Liu − *Department of NanoEngineering, University of California San Diego, La Jolla, California 92093, United States;* orcid.org/0000-0002-1488-1668; Email: piliu@eng.ucsd.edu

Authors

  John Holoubek − *Department of NanoEngineering, University of California San Diego, La Jolla, California 92093, United States;* orcid.org/0000-0003-0015-4512

  Haodong Liu − *Department of NanoEngineering, University of California San Diego, La Jolla, California 92093, United States*

  Qizhang Yan − *Department of NanoEngineering, University of California San Diego, La Jolla, California 92093, United States;* orcid.org/0000-0002-3798-642X

  Zhaohui Wu − *Department of NanoEngineering, University of California San Diego, La Jolla, California 92093, United States*

  Bao Qiu − *Ningbo Institute of Materials Technology and Engineering (NIMTE), Chinese Academy of Sciences, Zhejiang 315201, China;* orcid.org/0000-0002-7505-6135

  Minghao Zhang − *Department of NanoEngineering, University of California San Diego, La Jolla, California 92093, United States*

  Sicen Yu − *Department of NanoEngineering, University of California San Diego, La Jolla, California 92093, United States*

  Shen Wang − *Department of NanoEngineering, University of California San Diego, La Jolla, California 92093, United States;* orcid.org/0000-0003-3826-4397

  Jianbin Zhou − *Department of NanoEngineering, University of California San Diego, La Jolla, California 92093, United States*

  Tod A. Pascal − *Department of NanoEngineering, University of California San Diego, La Jolla, California 92093, United States;* orcid.org/0000-0003-2096-1143

  Jian Luo − *Department of NanoEngineering, University of California San Diego, La Jolla, California 92093, United States*

  Zhaoping Liu − *Ningbo Institute of Materials Technology and Engineering (NIMTE), Chinese Academy of Sciences, Zhejiang 315201, China;* orcid.org/0000-0002-3943-8953

  Ying Shirley Meng − *Department of NanoEngineering, University of California San Diego, La Jolla, California 92093, United States;* orcid.org/0000-0001-8936-8845

Complete contact information is available at:
https://pubs.acs.org/10.1021/acsami.3c07224

Author Contributions

[†]J.H., H.L., and Q.Z. contributed equally to this work. H.L. and P.L. conceived of the original idea. J.H., H.L., and Q.Z. conducted the experiments. J.H. conducted the computational simulations under the guidance of T.A.P. J.H., Q.Z., Z.W., S.Y., S.W., and J.Z. assisted with characterization and data analysis. B.Q. and Z.P. assisted with materials synthesis. J.L. and Y.S.M contributed resources and facilities. P.L. directed the project. J.H., H.L., Q.Z., and P.L. wrote the manuscript. All authors discussed the results and edited the manuscript.

Notes

The authors declare no competing financial interest.

ACKNOWLEDGMENTS

■ REFERENCES

(1) Liu, J.; Bao, Z.; Cui, Y.; Dufek, E. J.; Goodenough, J. B.; Khalifah, P.; Li, Q.; Liaw, B. Y.; Liu, P.; Manthiram, A.; Meng, Y. S.; Subramanian, V. R.; Toney, M. F.; Viswanathan, V. V.; Whittingham, M. S.; Xiao, J.; Xu, W.; Yang, J.; Yang, X.-Q.; Zhang, J.-G. Pathways for Practical High-Energy Long-Cycling Lithium Metal Batteries. *Nat. Energy* **2019**, *4* (3), 180−186.

(2) Yang, Z.; Huang, H.; Lin, F. Sustainable Electric Vehicle Batteries for a Sustainable World: Perspectives on Battery Cathodes, Environment, Supply Chain, Manufacturing, Life Cycle, and Policy. *Adv. Energy Mater.* **2022**, *12* (26), No. 2200383.

(3) Schmuch, R.; Wagner, R.; Hörpel, G.; Placke, T.; Winter, M. Performance and Cost of Materials for Lithium-Based Rechargeable Automotive Batteries. *Nat. Energy* **2018**, *3* (4), 267−278.

(4) Xu, P.; Tan, D. H. S.; Chen, Z. Emerging Trends in Sustainable Battery Chemistries. *Trends Chem.* **2021**, *3* (8), 620−630.

(5) Zuo, W.; Luo, M.; Liu, X.; Wu, J.; Liu, H.; Li, J.; Winter, M.; Fu, R.; Yang, W.; Yang, Y. Li-Rich Cathodes for Rechargeable Li-Based Batteries: Reaction Mechanisms and Advanced Characterization Techniques. *Energy Environ. Sci.* **2020**, *13* (12), 4450−4497.

(6) He, W.; Guo, W.; Wu, H.; Lin, L.; Liu, Q.; Han, X.; Xie, Q.; Liu, P.; Zheng, H.; Wang, L.; Yu, X.; Peng, D.-L. Challenges and Recent Advances in High Capacity Li-Rich Cathode Materials for High Energy Density Lithium-Ion Batteries. *Adv. Mater.* **2021**, *33* (50), No. 2005937.

(7) House, R. A.; Marie, J.-J.; Pérez-Osorio, M. A.; Rees, G. J.; Boivin, E.; Bruce, P. G. The Role of O2 in O-Redox Cathodes for Li-Ion Batteries. *Nat. Energy* **2021**, *6* (8), 781−789.

(8) House, R. A.; Maitra, U.; Pérez-Osorio, M. A.; Lozano, J. G.; Jin, L.; Somerville, J. W.; Duda, L. C.; Nag, A.; Walters, A.; Zhou, K.-J.; Roberts, M. R.; Bruce, P. G. Superstructure Control of First-Cycle Voltage Hysteresis in Oxygen-Redox Cathodes. *Nature* **2020**, *577* (7791), 502−508.

(9) Chen, D.; Kan, W. H.; Chen, G. Understanding Performance Degradation in Cation-Disordered Rock-Salt Oxide Cathodes. *Adv. Energy Mater.* **2019**, *9* (31), No. 1901255.

(10) Wu, H.; Dong, J.; Zhang, Y.; Lin, L.; Gao, G.; Li, T.; Yi, X.; Sa, B.; Wang, J.; Wang, L.; et al. Lattice Oxygen Redox Reversibility Modulation in Enhancing the Cycling Stability of Li-Rich Cathode Materials. *Adv. Funct. Mater.* **2023**, No. 2303707.

(11) Cui, C.; Fan, X.; Zhou, X.; Chen, J.; Wang, Q.; Ma, L.; Yang, C.; Hu, E.; Yang, X.-Q.; Wang, C. Structure and Interface Design Enable Stable Li-Rich Cathode. *J. Am. Chem. Soc.* **2020**, *142* (19), 8918−8927.

(12) Zhang, X.; Jia, H.; Xu, Y.; Zou, L.; Engelhard, M. H.; Matthews, B. E.; Wang, C.; Zhang, J.-G.; Xu, W. Unravelling High-Temperature Stability of Lithium-Ion Battery with Lithium-Rich Oxide Cathode in Localized High-Concentration Electrolyte. *J. Power Sources Adv.* **2020**, *5*, No. 100024.

(13) Qiu, B.; Zhang, M.; Wu, L.; Wang, J.; Xia, Y.; Qian, D.; Liu, H.; Hy, S.; Chen, Y.; An, K.; Zhu, Y.; Liu, Z.; Meng, Y. S. Gas−Solid Interfacial Modification of Oxygen Activity in Layered Oxide Cathodes for Lithium-Ion Batteries. *Nat. Commun.* **2016**, *7* (1), 12108.

(14) Cheng, X.-B.; Zhang, R.; Zhao, C.-Z.; Zhang, Q. Toward Safe Lithium Metal Anode in Rechargeable Batteries: A Review. *Chem. Rev.* **2017**, *117* (15), 10403−10473.

(15) Ren, X.; Zou, L.; Jiao, S.; Mei, D.; Engelhard, M. H.; Li, Q.; Lee, H.; Niu, C.; Adams, B. D.; Wang, C.; Liu, J.; Zhang, J.-G.; Xu, W. High-Concentration Ether Electrolytes for Stable High-Voltage Lithium Metal Batteries. *ACS Energy Lett.* **2019**, *4* (4), 896−902.

(16) Jiao, S.; Ren, X.; Cao, R.; Engelhard, M. H.; Liu, Y.; Hu, D.; Mei, D.; Zheng, J.; Zhao, W.; Li, Q.; Liu, N.; Adams, B. D.; Ma, C.; Liu, J.; Zhang, J.-G.; Xu, W. Stable Cycling of High-Voltage Lithium Metal Batteries in Ether Electrolytes. *Nat. Energy* **2018**, *3* (9), 739.

(17) Chen, S.; Zheng, J.; Mei, D.; Han, K. S.; Engelhard, M. H.; Zhao, W.; Xu, W.; Liu, J.; Zhang, J.-G. High-Voltage Lithium-Metal Batteries Enabled by Localized High-Concentration Electrolytes. *Adv. Mater.* **2018**, *30* (21), No. 1706102.

(18) Ren, X.; Zou, L.; Cao, X.; Engelhard, M. H.; Liu, W.; Burton, S. D.; Lee, H.; Niu, C.; Matthews, B. E.; Zhu, Z.; Wang, C.; Arey, B. W.; Xiao, J.; Liu, J.; Zhang, J.-G.; Xu, W. Enabling High-Voltage Lithium-Metal Batteries under Practical Conditions. *Joule* **2019**, *3* (7), 1662−1676.

(19) Cao, X.; Jia, H.; Xu, W.; Zhang, J.-G. Review—Localized High-Concentration Electrolytes for Lithium Batteries. *J. Electrochem. Soc.* **2021**, *168* (1), No. 010522.

(20) Holoubek, J.; Kim, K.; Yin, Y.; Wu, Z.; Liu, H.; Li, M.; Chen, A.; Gao, H.; Cai, G.; Pascal, T. A.; Liu, P.; Chen, Z. Electrolyte Design Implications of Ion-Pairing in Low-Temperature Li Metal Batteries. *Energy Environ. Sci.* **2022**, *15* (4), 1647−1658.

(21) Yoshida, K.; Nakamura, M.; Kazue, Y.; Tachikawa, N.; Tsuzuki, S.; Seki, S.; Dokko, K.; Watanabe, M. Oxidative-Stability Enhancement and Charge Transport Mechanism in Glyme−Lithium Salt Equimolar Complexes. *J. Am. Chem. Soc.* **2011**, *133* (33), 13121−13129.

(22) Suo, L.; Borodin, O.; Gao, T.; Olguin, M.; Ho, J.; Fan, X.; Luo, C.; Wang, C.; Xu, K. Water-in-Salt" Electrolyte Enables High-Voltage Aqueous Lithium-Ion Chemistries. *Science* **2015**, *350* (6263), 938−943.

(23) Perez Beltran, S.; Cao, X.; Zhang, J.-G.; Balbuena, P. B. Localized High Concentration Electrolytes for High Voltage Lithium−Metal Batteries: Correlation between the Electrolyte Composition and Its Reductive/Oxidative Stability. *Chem. Mater.* **2020**, *32* (14), 5973−5984.

(24) Perez Beltran, S.; Cao, X.; Zhang, J.-G.; El-Khoury, P. Z.; Balbuena, P. B. Influence of Diluent Concentration in Localized High Concentration Electrolytes: Elucidation of Hidden Diluent-Li+ Interactions and Li+ Transport Mechanism. *J. Mater. Chem. A* **2021**, *9* (32), 17459−17473.

(25) Fan, X.; Chen, L.; Borodin, O.; Ji, X.; Chen, J.; Hou, S.; Deng, T.; Zheng, J.; Yang, C.; Liou, S.-C.; Amine, K.; Xu, K.; Wang, C. Non-Flammable Electrolyte Enables Li-Metal Batteries with Aggressive Cathode Chemistries. *Nat. Nanotechnol.* **2018**, *13* (8), 715.

(26) Cao, X.; Ren, X.; Zou, L.; Engelhard, M. H.; Huang, W.; Wang, H.; Matthews, B. E.; Lee, H.; Niu, C.; Arey, B. W.; Cui, Y.; Wang, C.; Xiao, J.; Liu, J.; Xu, W.; Zhang, J.-G. Monolithic Solid−Electrolyte Interphases Formed in Fluorinated Orthoformate-Based Electrolytes Minimize Li Depletion and Pulverization. *Nat. Energy* **2019**, *4* (9), 796−805.

(27) Qian, J.; Henderson, W. A.; Xu, W.; Bhattacharya, P.; Engelhard, M.; Borodin, O.; Zhang, J.-G. High Rate and Stable Cycling of Lithium Metal Anode. *Nat. Commun.* **2015**, *6*, 6362.

(28) Cheng, H.; Sun, Q.; Li, L.; Zou, Y.; Wang, Y.; Cai, T.; Zhao, F.; Liu, G.; Ma, Z.; Wahyudi, W.; Li, Q.; Ming, J. Emerging Era of Electrolyte Solvation Structure and Interfacial Model in Batteries. *ACS Energy Lett.* **2022**, *7*, 490−513.

(29) Amanchukwu, C. V.; Kong, X.; Qin, J.; Cui, Y.; Bao, Z. Nonpolar Alkanes Modify Lithium-Ion Solvation for Improved Lithium Deposition and Stripping. *Adv. Energy Mater.* **2019**, *9* (41), No. 1902116.

(30) Xu, H.; Zhang, J.; Zhang, H.; Long, J.; Xu, L.; Mai, L. In Situ Topological Interphases Boosting Stable Solid-State Lithium Metal Batteries. *Adv. Energy Mater.* **2023**, *13* (21), No. 2204411.

(31) Fadel, E. R.; Faglioni, F.; Samsonidze, G.; Molinari, N.; Merinov, B. V.; Goddard, W. A., III; Grossman, J. C.; Mailoa, J. P.; Kozinsky, B. Role of Solvent-Anion Charge Transfer in Oxidative Degradation of Battery Electrolytes. *Nat. Commun.* **2019**, *10* (1), 3360.

(32) Xu, K. Electrolytes and Interphases in Li-Ion Batteries and Beyond. *Chem. Rev.* **2014**, *114* (23), 11503−11618.

(33) Li, Y.; Li, Y.; Pei, A.; Yan, K.; Sun, Y.; Wu, C.-L.; Joubert, L.-M.; Chin, R.; Koh, A. L.; Yu, Y.; Perrino, J.; Butz, B.; Chu, S.; Cui, Y. Atomic Structure of Sensitive Battery Materials and Interfaces Revealed by Cryo−Electron Microscopy. *Science* **2017**, *358* (6362), 506−510.

(34) Zhang, Z.; Yang, J.; Huang, W.; Wang, H.; Zhou, W.; Li, Y.; Li, Y.; Xu, J.; Huang, W.; Chiu, W.; Cui, Y. Cathode-Electrolyte Interphase in Lithium Batteries Revealed by Cryogenic Electron Microscopy. *Matter* **2021**, *4* (1), 302−312.

(35) Xiao, X.; Wang, L.; Li, J.; Zhang, B.; Hu, Q.; Liu, J.; Wu, Y.; Gao, J.; Chen, Y.; Song, S.; Zhang, X.; Chen, Z.; He, X. Rational Synthesis of High-Performance Ni-Rich Layered Oxide Cathode Enabled via Probing Solid-State Lithiation Evolution. *Nano Energy* **2023**, *113*, No. 108528.

(36) Jung, S.-K.; Gwon, H.; Hong, J.; Park, K.-Y.; Seo, D.-H.; Kim, H.; Hyun, J.; Yang, W.; Kang, K. Understanding the Degradation Mechanisms of LiNi0.5Co0.2Mn0.3O2 Cathode Material in Lithium Ion Batteries. *Adv. Energy Mater.* **2014**, *4* (1), No. 1300787.

(37) Lin, F.; Markus, I. M.; Nordlund, D.; Weng, T.-C.; Asta, M. D.; Xin, H. L.; Doeff, M. M. Surface Reconstruction and Chemical Evolution of Stoichiometric Layered Cathode Materials for Lithium-Ion Batteries. *Nat. Commun.* **2014**, *5* (1), 3529.

(38) Langdon, J.; Sim, R.; Manthiram, A. Gas Generation in Lithium Cells with High-Nickel Cathodes and Localized High-Concentration Electrolytes. *ACS Energy Lett.* **2022**, *7* (8), 2634−2640.